Published in final edited form as:
Nat Cell Biol. 2011 March ; 13(3): 203–214. doi:10.1038/ncb2163.

Developmental roles for Srf, cortical cytoskeleton and cell shape in epidermal spindle orientation

Chen Luxenburg[1], **H. Amalia Pasolli**[1], **Scott E. Williams**[1], and **Elaine Fuchs**[1,2]

[1]Howard Hughes Medical Institute, Laboratory of Mammalian Cell Biology and Development, The Rockefeller University, New York, New York 10065, USA

Abstract

During development, a polarized epidermal sheet undergoes stratification and differentiation to produce the skin barrier. Through mechanisms that are poorly understood, the process involves actin dynamics, spindle reorientation and Notch signalling. To elucidate how epidermal embryogenesis is governed, we conditionally targeted serum response factor (Srf), a transcription factor that is essential for epidermal differentiation. Unexpectedly, previously ascribed causative defects are not responsible for profoundly perturbed embryonic epidermis. Seeking the mechanism for this, we identified actins and their regulators that were downregulated after ablation. Without Srf, cells exhibit a diminished cortical network and in mitosis, they fail to round up, features we recapitulate with low-dose actin inhibitors *in vivo* and shRNA-knockdown *in vitro*. Altered concomitantly are phosphorylated ERM and cortical myosin-IIA, shown *in vitro* to establish a rigid cortical actomyosin network and elicit critical shape changes. We provide a link between these features and Srf loss, and we show that the process is physiologically relevant in skin, as reflected by defects in spindle orientation, asymmetric cell divisions, stratification and differentiation.

Epidermis is an ideal paradigm for studying how tissue architecture is achieved and how established tissues maintain homeostasis by balancing growth and differentiation. Loss-of-function studies have revealed fundamental roles for adherens junctions and focal adhesions in generating the requisite polarity necessary for embryonic epidermis to stratify and differentiate[1,2]. Also important in establishing architecture is the orientation of mitotic spindles, which change from lateral to perpendicular orientations concomitant with stratification[3].

Several lines of mostly *in vitro* evidence indicate that the cortical cytoskeleton participates in structurally organizing and positioning mitotic spindles[4,5]. As cells go through mitosis, they alter their geometry, a process involving massive actin remodelling and redistribution of cortical proteins[6–10]. In *Caenorhabditis elegans* zygotes, reorganization of cortical actomyosin on sperm entry establishes polarity that guides spindle orientation[11–14]. In fertilized mouse oocytes, cortical tension affects spindle structure and rotation[15]. Relations between the molecular composition of cortex, cell shape and spindle orientation have not

[2]Correspondence should be addressed to (fuchslb@rockefeller.edu) .

Note: Supplementary Information is available on the Nature Cell Biology website

AUTHOR CONTRIBUTIONS C.L. and H.A.P. carried out the experiments and analysed the raw data. S.E.W. contributed reagents and experimental suggestions. C.L. and E.F. wrote the manuscript. E.F. supervised the project.

COMPETING FINANCIAL INTERESTS The authors declare no competing financial interests.

been studied in the context of a complex tissue such as mouse epidermis, where spindle orientation is critical to achieve tissue form and function.

We were intrigued by studies in which Srf, a ubiquitous transcription factor, was conditionally targeted in the epidermis, yielding an imbalance in proliferation and differentiation[16,17]. These defects have been attributed to various processes, including enhanced inflammation[17] and/or disrupted cell–cell adhesion[16]. In cultured keratinocytes, Srf activates *Fos* and *Junb* to promote terminal differentiation *in vitro*[18]. That said, Srf regulates many genes, including regulators of actin cytoskeleton, adhesion and contractility[19,20]. Moreover, *in vivo* studies of muscles[21,22], forebrain[23], endothelium[24] and metastasis[25] emphasize roles for Srf in contractility, migration and adhesion. With increasing evidence that actin dynamics function in epidermal stratification and differentiation, it seemed important to explore whether Srf has additional roles in regulating tissue development. In the present study, we show that when Srf is missing during epidermal morphogenesis, defects in actin dynamics precede the myriad of other alterations attributable to Srf loss. In pursuing the physiological relevance, we discovered that when normal epidermal cells enter mitosis, they reinforce their actomyosin cortical network, but soon after *Srf* ablation, this process is disabled. We show that this mechanism is critical for mitotic basal cells to adopt necessary shape changes to properly localize leucine–glycine–asparagine repeat-enriched protein (LGN) and nuclear mitotic apparatus protein (NuMA) and reorient their spindle, so that stratification and differentiation can be achieved. The ability of Srf to orchestrate this process unveils a previously unknown role for this broadly expressed transcription factor.

RESULTS

Srf-deficiency alters the basal to suprabasal transition

Conditional targeting of *Srf* was achieved by breeding *Srf* fl/fl mice[21] to mice expressing *Keratin(K)-14* promoter-driven Cre recombinase[26]. Nuclear Srf protein was uniformly lost by embryonic day 16.5 (E16.5; Fig. 1a). Mice conditionally null for *Srf* (cKO) died within 24 h. Newborn cKO animals were runted, and exhibited open eyes, as reported previously[16].

Heterozygous or wild-type E16.5 epidermis consists of an inner layer of polarized basal cells overlaid by differentiating, keratin-rich spinous cells, granular cells and surface stratum corneum (Fig. 1b). In contrast, Srf-deficient basal cells were often located between basal and spinous layers or within the spinous layer (Fig. 1b). As development proceeded, cellular organization became increasingly perturbed (Fig. 1b and Supplementary Fig. S1).

Differentiation and proliferation defects emerge subsequent to morphological changes, but before inflammation

The basal to spinous differentiation switch in wild-type epidermis is accompanied by repression of basal keratins K14/K5 and induction of spinous keratins K1/K10 (ref. 27), whereas suprabasal activation of K6/K16 typically reflects an imbalance in normal homeostasis[28]. In *Srf*-cKO epidermis, keratin expression was markedly perturbed. This was most obvious from E17.5 onward, where K5/K14 extended suprabasally and K6/K16 replaced K1/K10 in most spinous cells (Fig. 2a–c). Immunoblot analyses confirmed these alterations (Fig. 2d), providing an ~1 day delay in the molecular explanation for the blurred ultrastructural basal to spinous layer distinction.

Differentiation depends on Notch signalling, which leads to suprabasal activation of downstream target genes, such as *Hes1* (refs 29–33). Immunolocalization for Notch receptor and nuclear Hes1 was normal at E16.5, but by E17.5, both Notch and Hes1 were repressed in *Srf*-cKO when compared with wild-type epidermis (Fig. 2e,f). These aberrations occurred

concurrently with biochemical changes, but subsequent to Srf-deficiency and morphological anomalies. At E17.5, increases in actively cycling cells were also detected. Notably, this timing coincided with K14+ cell expansion and repressed differentiation. Differences in cycling cells were most evident suprabasally and seemed to be counterbalanced by elevated apoptosis (Supplementary Fig. S2).

Proliferation and differentiation imbalances were also noted in adult animals exhibiting spontaneous *Srf* ablation. In that case, defects were traced to accompanying inflammation[17]. In contrast, even though skins from *K14–Cre* newborn *Srf*-cKO pups exhibited an ~4× increase in CD45-positive immune cells and ~9× increase in Mac1-positive macrophages, immune infiltration was not detected at E16.5–E17.5 (Supplementary Fig. S3). Hence, embryonic differentiation defects elicited by Srf deficiency were not attributable to inflammation.

Srf-mediated perturbations in adhesion and apicobasal polarity emerge subsequent to morphological changes

Alterations in differentiation, hyperproliferation and apoptosis were reported in severely affected newborn mice lacking Srf. In that case and in adults, loss of cell adhesion was thought to be a major contributing factor[16,17]. However, embryonic *Srf*-cKO epidermis still had E-cadherin at its (irregular) intercellular borders (Fig. 3a). By birth, E-cadherin levels were actually elevated (Fig. 3a,b). Similar results were obtained for other core components of adherens junctions and desmosomal–keratin networks (Supplementary Fig. S4). In addition, despite some suprabasal localization, cell–substratum components seemed largely unperturbed.

Ultrastructurally, intercellular membranes were sealed and both hemidesmosomes and desmosomes and their keratin filament connections seemed to be intact in Srf-deficient embryonic skin. Even at birth, the basal layer of *Srf*-cKO and wild-type pups exhibited similar lengths of membrane occupied by hemidesmosomes (0.35 ± 0.05 wild type, 0.32 ± 0.02 cKO). The membrane length occupied by desmosomes was actually elevated in Srf-deficient cells (0.044±0.003 wild type, 0.09±0.01 cKO; Fig. 3c,d), although individual desmosome size was not affected (0.24±0.05 μm wild type, 0.24±0.01 μm cKO). Surprisingly, cell adhesion was not disrupted even in places where the morphology of newborn epidermis was grossly altered and many cells were filled with large vacuoles (Supplementary Fig. S1). On the basis of these findings, we conclude that early Srf loss does not cripple embryonic epidermal adhesion.

Although not sufficient for establishing apicobasal polarity (ABP), intercellular and cell–substratum adhesion are prerequisites. At E16.5, two key ABP features were properly localized apically in Srf-deficient skin: Par3 and centrosomes[3] (Fig. 3e,f). By E17.5, concomitant signs of altered ABP and terminal differentiation were apparent. By E18.5, polarity was grossly disturbed. Overall, ABP perturbations appeared ~1 day following Srf loss and morphological irregularities. We revisit the sequential appearance of these events later.

Srf-deficiency in skin embryogenesis leads to early transcriptional changes involving predominantly, but not exclusively, actin regulators

To gain insights into the early morphological abnormalities that accompany Srf loss, we turned to transcriptional profiling. We made *K14–Cre* × *Srf(fl/fl)* × *Rosa26–fl–stop–fl–YFP* mice and used fluorescence activated cell sorting (FACS) to purify Cre-activated basal cells (YFP^+ $\alpha6$-$integrin^+$) from control and cKO E16.5 embryos (Supplementary Fig. S5a). These

populations were then used for microarray analyses, which were then validated by real-time PCR (Fig. 4a; Table 1 and Supplementary Fig. S5b).

At these early times after *Srf* targeting, only 72 messenger RNAs scored as down-(49) or up-(23) regulated >1.5 fold (*P* value < 0.05; Supplementary Tables S1 and S2). As revealed by the functional annotation-clustering algorithm 'DAVID'[34], downregulated genes were clustered into 'actomyosin cytoskeleton' (*P* value=2.2×10^{-4}; Table 1). These included fundamental F-actin building blocks (*β, γ-actin*; *Actb, Actg1*; refs 20,35); an F-actin stabilizer (H2-calponin, *Cnn2*; refs 36–38); F-actin crosslinkers (FilaminA, *Flna*; Filamin-binding LIM protein 1, *Fblim1*; ref. 39) and an actin-interacting protein 1 (*Wdr1*) that can influence severing activity and mediate cell shape changes associated with mitosis *in vitro*[40]. Other actin regulators Gelsolin (*Gsn*) and Profilin 2 (*Pfn2*), which regulate severing/capping and polymerization, respectively, were also downregulated, albeit with a lower-fold change.

Despite the absence of overt differences in cellular junctions, early Srf-mediated changes included intercellular adhesion/signalling genes (*Dsg1a, Dsg1b, Gjb5, Pcdh20*), and a cell–substratum gene (*Tns4*). In contrast, transcripts associated with Notch signalling and other transcriptional regulators of epidermal differentiation seemed unaffected by early loss of Srf, as did genes involving ABP and inflammation (Table 1 and Supplementary Fig. S5b).

The highest-fold changes were in established Srf targets *Egr1-3*, which encode transcription factors that function as tumour suppressors in many tissues, including skin[41]. However, E16.5 SRF-deficient epidermis was not hyperproliferative, and only one cell-cycle-regulatory gene, *Ccnd2*, was upregulated in our array. Moreover, *Nab2*, a known target of *Egr1-3* (ref. 42), was unchanged and *Gadd45a/b*, which are positively regulated by Egr1 in epidermis[42–44], were not downregulated in E16.5 *Srf* -null basal cells (Table 1 and Supplementary Fig. S5b). Thus, consequences of *Egr* downregulation seemed to arise subsequent to E16.5, similarly to enhanced proliferation (Supplementary Fig. S2).

Finally, neither *Fos* nor *Junb* showed appreciable change in our E16.5 array and quantitative PCR (qPCR; Supplementary Fig. S5b). Thus, although these genes are well known Srf targets and they function critically in regulating keratinocyte differentiation *in vitro*[18], they did not seem to contribute substantially to the earliest morphological changes arising in Srf-deficient skin.

Srf-mediated alterations in cortical actin occur early and result in a failure of mitotic cells to round up

Collectively, these data pointed to alterations in actomyosin cytoskeletal genes as the source of basal to spinous defects in *Srf* -null E16.5 embryos. Indeed, although cortical actin cytoskeleton was still present, its intensity was diminished to 45±11% of wild-type basal cell levels (Fig. 4b,c). This defect was accentuated with age, showing nearly complete loss of cortical actin by E18.5 (Supplementary Fig. S6).

In vitro studies show that the actin cytoskeleton is remodelled when cells enter and progress through mitosis; this process is thought to allow cells to round up and generate cortical actomyosin tension to facilitate division[4,10,45]. To test whether embryonic basal cells round up in mitosis and whether this is compromised on *Srf* ablation, we imaged cells through the plane of the E16.5 basal layer (Fig. 4d). We used a higher exposure to illuminate the otherwise reduced cortical actin network, so we could quantify cell shapes in cKO tissue. Although some heterogeneity existed, the average axial ratio of wild-type basal cells went from 1.59±0.06 in interphase to 1.10±0.01 in early mitosis. This ratio was largely unchanged in cKO basal cells (1.51±0.05, interphase versus 1.40±0.08, mitosis; Fig. 4e), reflecting an inability to undergo proper shape changes during mitosis.

Wild-type embryos exposed to actin inhibitors phenocopy the failure of *Srf* -null basal cells to undergo shape changes during mitosis

To test whether actin perturbations account for the observed phenotypic changes seen in *Srf*-cKO E16.5 embryos, we treated wild-type embryos with latrunculin, which specifically inhibits actin polymerization[46,47]. To mimic early stages of Srf loss, we first showed that after mild exposure of wild-type E14.5 embryos to latrunculin (0.25 μM), ABP was still intact, and cortical actin was only reduced, not abolished (Fig. 4f–h). This treatment seemed to impair rounding of mitotic basal cells more than it affects interphase cell shape (Fig. 4i,j). Our findings on embryos agree with previous reports that PtK2 cells fail to round up during mitosis following exposure to actin inhibitors[10]. We will return to this issue later.

Srf-cKO early mitotic cells fail to activate ERM proteins and recruit myosin-IIA to their cortices

Thus far, our studies pointed to a sensitivity of mitotic basal cells to Srf loss and to its accompanying diminution of cortical actin. Recent *in vitro* studies showed that the single *Drosophila* ERM (Ezrin–Radixin–Moesin) protein undergoes phosphorylation during mitosis[6,7]. This event is thought to trigger cell rounding, cortical stiffening and myosin-II recruitment required to progress through cell division. In light of our findings, we examined whether this mechanism is operative in E16.5 mouse epidermis, and whether it is compromised as an early consequence of *Srf* ablation.

Immunofluorescence microscopy revealed an enrichment of ERM proteins at intercellular borders of wild-type, but not *Srf* -null, basal cells (Fig. 5a). Moreover, whereas early mitotic cells of wild-type epidermis exhibited strong phospho-ERM immunolabelling at the cortex, *Srf* -null counterparts showed weaker and discontinuous labelling (Fig. 5b,c). Consistent with our array and qPCR data, immunoblot analyses revealed similar ERM levels, but reduced phosphorylated ERM in cKO versus wild-type P0 epidermis (Fig. 5d). This difference seemed to result from Srf-mediated alterations in cortical actin, because exposing embryos to low latrunculin reduced numbers of mitotic cells with enriched cortical phosphorylated ERM (Fig. 5e).

Planar imaging of E16.5 wild-type embryos also revealed enhanced myosin-IIA at the cortex of rounded, mitotic cells (Fig. 5f). Similarly to phospho-ERM, this enrichment was abolished in *Srf*-cKO epidermis, along with shape changes that typically accompany mitotic cells. These differences were not attributable to the particular imaging plane, as verified by merging collective *Z* -stack images of mitotic basal cells (insets).

Quantifications of fluorescence intensity ratios of both wild-type and *Srf*-cKO skins showed that cortical F-actin intensities were comparable between mitotic cells and their non-mitotic neighbours (Fig. 5g). In contrast to wild-type cells, however, the >3-fold enrichment of myosin-IIA intensity at the mitotic cortex did not occur in *Srf* -null cells (Fig. 5g). Similar to our observations with ERM, overall levels of myosin mRNAs and proteins were not affected by early Srf loss (Fig. 5h and Supplementary Fig. S5b). Moreover, as observed in moesin-depleted cells[6,7], myosin-IIA was readily detectable at the midzone of late mitotic cells, and binucleated cells were not detected (Supplementary Fig. S7). Thus, the defect seemed to be primarily in myosin-IIA cortical recruitment, rather than cleavage furrow recruitment. Similar to Srf loss, latrunculin resulted in discontinuous and diminished myosin-IIA at the mitotic cortex (Fig. 5i,j).

Srf-mediated changes in actin-related proteins are sufficient to account for the failure to activate ERM proteins, recruit myosin-IIA and undergo mitotic cell shape changes

To explore Srf-mediated regulation of actin genes further, we tested the effects of knocking down their mRNAs on mitotic shape. When plated on collagen/fibronectin-coated coverslips for 18 h, wild-type keratinocytes formed a nearly confluent monolayer, which then assembled into an adherent sheet on calcium elevation. Nocodazole exposure arrested mitotic keratinocytes for image analyses (Fig. 6a, left).

With this *in vitro* system, we first documented a recapitulation of our low-latrunculin *in vivo* phenotype. Mitotic stage was identified by chromatin structure (4,6-diamidino-2-phenylindole, DAPI), and cell shape was delineated by cortical phospho-ERM and F-actin (phalloidin; Fig. 6a). In contrast to control (dimethylsulphoxide, DMSO)-treated cultures, 0.25 μM latrunculin perturbed the cortical distribution of pERM proteins and myosin-IIA in mitotic cells (Fig. 6a). Although total cell area was not affected, axial ratio quantifications indicated that latrunculin-treated mitotic cells failed to round up (1.26±0.23, DMSO versus 1.47±0.37, latrunculin; Fig. 6a–c).

Next, focusing on *β-actin* and *Wdr1*, we identified suitable shRNAs that when compared with scramble shRNA controls, diminished mRNA and protein levels (Fig. 6d,e). Phenotypically, mitotic keratinocytes expressing scramble shRNAs were indistinguishable from their uninfected or DMSO-treated counterparts (Fig. 6f).

Mitotic cells expressing *Actb* shRNAs failed to round up, and exhibited diminished cortical actin (Fig. 6f–j). Most importantly, although phospho-ERM cortical intensity remained high, its distribution was uneven and myosin-IIA cortical recruitment was affected. Mitotic keratinocytes expressing *Wdr1* shRNAs also failed to round up[40], but in contrast to the *Actb* shRNA, cortical phospho-ERM was significantly reduced (Fig. 6f,h). Wdr1-deficient keratinocytes were flat, precluding quantification of F-actin and myosin-IIA levels; however, they did not exhibit the typical cortical enrichment of these proteins.

Together, these findings indicate that both β-actin and Wdr1 contribute to the ability of mitotic keratinocytes to round up. A decrease in β-actin affected pERM distribution, and alterations in Wdr1 altered ERM phosphorylation (activation). Downstream to ERM activation, myosin-IIA recruitment was sensitive to the knockdown of either mRNA. Although beyond the scope of the present study, these data underscore the relevance of our array data, and indicate that multiple Srf-regulated genes may collaborate to govern the cortical actomyosin dynamics necessary to undergo proper basal cell divisions in developing epidermis.

ERM phosphorylation and mitotic cell shape changes function in spindle orientation and asymmetric cell divisions

In *Drosophila* cells, the failure to undergo ERM-actomyosin-induced cortical shape changes during mitosis results in structurally abnormal spindles with unstable localization[6,7]. Although spindles seemed largely intact within E16.5 Srf-deficient epidermis, their orientation was grossly perturbed (Fig. 7a,b). In contrast to basal divisions in wild-type embryos where >70% were perpendicular to the underlying basement membrane[3], <20% of divisions were perpendicular in *Srf*-cKO skin. Moreover, whereas <5% of wild-type basal cells divided at an oblique angle, ~50% of dividing *Srf* -deficient cells exhibited intermediate spindle angles.

Perpendicularly oriented spindles in stratifying embryonic epidermis are accompanied by an apical crescent of cortical LGN and NuMA (ref. 3). These proteins are thought to connect astral microtubules of one spindle pole to the apical cortex[48–52]. Srf loss did not alter *Gpsm2*

(LGN) or *NuMA1* (NuMA) mRNA levels, nor did it affect the percentage of LGN+ cells (Fig. 7c,d). However, the orientation of the LGN–NuMA cortical crescent was randomized in Srf-deficient mitotic cells (Fig. 7e,f).

We used double-immunofluorescence microscopy to position LGN–NuMA and spindle orientation in the cascade of events that follow Srf deficiency. When apical positioning of the Par3 complex is compromised with mutants that affect adhesion, spindle orientations become random[3]. In Srf-deficient skin, however, randomization of LGN–NuMA and spindle orientation preceded perturbations in Par3 and centrosomal positioning (Fig. 7g,h).

As expected, LGN+ wild-type basal cells were also phospho-ERM+. However, both were perturbed in Srf-deficient E16.5 basal cells, concurrent with reduction in myosin-IIA enrichment (Fig. 7g). Finally, LGN and spindle orientation defects occurred in embryos treated with either of two drugs that affect actin dynamics, latrunculin and jasplakinolide[53], at doses and times that did not affect Par3 or centrosome positioning. Blebistatin, an inhibitor of myosin-II motor activity[54], also perturbed LGN distribution (Supplementary Fig. S8). Together these results place LGN–NuMA and spindle orientation as early events that accompany inabilities of mitotic cells to round up, activate ERM proteins and recruit myosin-IIA to their cortices (Fig. 7i).

DISCUSSION

In vitro studies show that as cells enter mitosis, they round in shape and stiffen their cortex[4,45], processes involving massive actin remodelling[10]. In *Drosophila*, the trigger is ERM phosphorylation, which reorganizes and links cortical actin fibres to plasma membrane, thereby facilitating myosin-II recruitment and achieving spherical morphology and tension necessary for cell division[6,7]. We have discovered that when basal epidermal cells in normal mouse embryos enter mitosis, they activate ERM proteins, triple myosin-IIA at their cortex and round up. In contrast, their *Srf* -null counterparts cannot generate a cortical platform compatible for ERM protein activation and myosin-IIA recruitment. Consequently, *Srf* -null cells fail to undergo shape changes that normally accompany these mitotic events. Our results now implicate Srf, and in so doing, we take these observations up the evolutionary kingdom and to an *in vivo* level.

Although Srf can regulate *Myh9* (Myosin-IIA) transcription[25], E16.5 Srf-deficient skin showed alterations primarily in actin regulators. Our actin-inhibitor and knockdown studies revealed the importance of these changes to actomyosin dynamics. Thus, our results best fit a model whereby Srf governs the transcriptional program that establishes cortical framework. Early mitosis-inducing post-translational modifications then function to reinforce the cortex and remodel cellular shape. These mechanisms have not been described before in epidermal development or homeostasis, nor has a role for Srf been found for cortical changes in ERM and myosin dynamics in mitotic cells of any tissue.

In culture, the biological significance of actomyosin perturbations is underscored by spindle defects and abnormal divisions that occur when cells fail to achieve proper shape, cortical organization and tension[4,6,7,9,45]. Importantly, in ERM-depleted cells, spindle structural defects are corrected when cortical stiffness is restored from the extracellular side[7], and spindle orientations are restored when unregulated contractility is suppressed[6]. During early cytokinesis, myosin-II responds to and ‘corrects’ shape deformations before completing cytokinesis[55].

It is tempting to speculate that at the embryo surface, enriching myosin-IIA at the mitotic cortex might serve as a mechanical buffer to protect spindle from undesirable cell-shape distortions. Mechanistically, we show that cortical actomyosin-derived signals are essential

not only for remodelling epidermal shape during mitosis, but also for spindle orientation. Furthermore, randomized spindle orientations arising after Srf targeting or actomyosin inhibitors highlights their acute sensitivity to changes in cortical actomyosin that influences cell shape. Whereas our studies show that Srf drives basal cell shape changes *in vivo*, it is intriguing that *in vitro*, it is the shape changes—from stretched and flattened to rounded—that induce Srf (ref. 18).

Our data indicate that cell shape, ERM protein activation and myosin-IIA cortical recruitment are critical for properly orientating the LGN–NuMA complex in mitotic keratinocytes. In lower eukaryotes, redistribution of myosin-II and cortical tension promote proper spindle orientation and asymmetric division[56–58], and recently, LGN/Pins (partner of inscuteable) was found to regulate myosin-II cortical distribution[56]. Interestingly, in these systems, cortical myosin-II was polarized, whereas in embryonic keratinocytes, myosin-IIA was distributed throughout cortex. Further explorations into how actomyosin dynamics function in asymmetric divisions should provide clues for the basis of these differences.

Spindle orientation and asymmetric inheritance have emerged as pivotal mechanisms that allow stem cells to balance self-renewal and differentiation in a directional manner[49,57]. Both Srf and the actomyosin cytoskeleton are sensitive to numerous cues that vary from chemical to mechanical[19,20,59,60]. Our observations indicate that these signals can be integrated through Srf and cortical actomyosin to regulate spindle orientation, asymmetric cell division, cell fate determination and differentiation. The mechanisms that we have revealed demonstrate a role for Srf in regulating these fundamental biological processes, and new insights into how epidermal divisions and tissue morphogenesis are achieved.

METHODS

Methods and any associated references are available in the online version of the paper at http://www.nature.com/naturecellbiology/

METHODS

Mouse lines and breeding

B6/129S6 Srf^{tm1Rmn}/J mice[21] were crossed to CD1 transgenic mice expressing Cre recombinase under the control of the human *keratin 14* promoter[26] to generate *Srf*(*fl*/+) ×*K14–Cre* animals. B6/129S6 Srf^{tm1Rmn}/J mice were also crossed to *ROSA26 fl–Stop–fl–YFP* animals[61] to generate a double-homozygous line. The two lines were crossed to generate *Srf*-cKO , *ROSA–YFP* mice. *Srf*(*fl*/+), *K14–Cre* and *Srf*(+/+),K14-Cre mice are referred to as wild type, as they were indistinguishable by the assays carried out.

Immunodetection and antibodies

Primary antibodies used were: Srf (1:500, Santa-Cruz), MIIA (1:500, Covance), E-cadherin (1:200, ECCD-1, M. Takeichi), CD104 (1:200, 4-integrin, BD-Pharmigen), P-cadherin (1:100, Pcad, Zymed), Desmoplakin (1:300, Research Diagnostics), K14 (1:500, Fuchs Lab), K10 (1:500, Fuchs Lab), K6 (1:500, Fuchs Lab), Ki67 (1:500 Novocastra), cleaved Caspase 3 (1:200, Cell Signaling), β- and α-catenin (1:200, Sigma), *β-actin* (1:5,000, Sigma), Vinculin (1:200, Sigma), MHC (1:1,000, Sigma), MLC (1:1,000, Sigma), HPRT (1:2,000, Abcam) PAR3 (1:200, Millipore), PC (1:500, Covance), Notch3 (1:200, Biologend), Hes1 (1:200, Fuchs Lab), pHH3 (1:500, Upstate), LGN (1:500, Fuchs Lab), NuMA (1:200, Cell Signaling), Ac-Tub (1:300, Sigma), CD3 (1:200 Chemicon), CD45 (1:200, BD-Pharmigen), Mac1 (1:200, BD-Pharmigen), BrdU (1:300, Abcam) ERM (1:200, Cell Signalling) and pERM (1:100, Cell Signalling). Secondary antibodies (1:500) were

conjugated to fluorescein isothiocyanate (FITC) or Texas red (The Jackson Labs) or biotin (Vector Labs). F-actin was labelled with Phalloidin-Alexa Fluor 546 (1:1,000, Invitrogen).

For tissue analyses, skins were frozen and embedded in optimal cutting temperature (OCT) compound or fixed overnight with buffered 4% formaldehyde at 4°C and embedded in paraffin. For immunoreactions, skin sections (10 μM) were blocked with PBS, 0.3% Triton X-100, 1% bovine serum albumin, 5% normal goat serum, 5% normal donkey serum or MOM Basic kit (Vector Labs). Primary antibodies were incubated for 1 h at room temperature or overnight at 4°C. Secondary antibodies were incubated at room temperature for 1 h. For whole-mount immunofluorescence microscopy, embryos were fixed for 1 h in 4% formaldehyde, and primary antibodies were incubated overnight at 4°C.

For immunoblots, skins were incubated in dispase for 12 h at 4°C, to selectively remove the epidermis, which was then frozen in liquid nitrogen and crushed. For immunoblot analyses, proteins were extracted and processed as described[62]. Samples were run on 4–12% gradient gels, transferred to nitrocellulose, and blotted overnight with the indicated antibodies.

Microscopy and image processing

Whole-mount images were acquired with a Zeiss LSM510 laser-scanning microscope (Carl Zeiss MicroImaging) through a ×100/1.4 oil objective. Images were recorded at 1,024× 1,024 square pixels. OCT immunofluorescence section images (10 μm) were acquired with a DeltaVision-RT system (Applied Precision), consisting of an inverted microscope IX71 equipped with ×60/1.42 oil or ×20/0.75 air objectives (Olympus). Red–green–blue images were assembled in Adobe Photoshop CS2 v. 9.0.2 and panels were labelled in Adobe Illustrator CS2 v. 12.0.1.

Electron microscopy

For transmission electron microscopy, samples were fixed in 2% glutaraldehyde, 4% paraformaldehyde and 2 mM CaCl2 in 0.05 M sodium cacodylate buffer, at pH 7.2, at room temperature for >1 h. Samples were post-fixed in 1% osmium tetroxide and processed for Epon embedding. Ultrathin sections (60–70 nm) were counterstained with uranyl acetate and lead citrate. Electron micrographs were taken with a transmission electron microscope (Tecnai G2-12; FEI) equipped with a digital camera (Model XR60; Advanced Microscopy Techniques).

FACS

FACS purification of basal epidermal cells from E16.5 *Srf fl/fl ROSA26 YFP fl/fl K14–Cre* (cKO) or *Srf fl/+ROSA26 YFP fl/fl K14–Cre* (wild type) mice was carried out on a FACS Vantage SE system equipped with FACS DiVa software (BD Biosciences). Cells were gated for single events and viability and then sorted according to phycoerythrin-conjugated α6-integrin expression and YFP fluorescence.

Microarray analysis

FACS-purified basal cells from the epidermis of wild-type and *Srf*-cKO E16.5 embryos were given to the MSKCC Genomics Core Facility for RNA extraction, quality control, quantification, reverse transcription, labelling, and hybridization to MOE430A 2.0 microarray chips (Affymetrix). Arrays were hybridized as per the manufacturer's specifications to Affymetrix MOE430v2 chips. Images were subtracted for background signals, and probe-set expression estimates were generated using the MAS5 algorithm implemented in the Bioconductor open software developed for computational biology and bioinformatics. A detection *P* value of $P \leq 0.05$ was used to set the threshold of probe sets into present ($P < 0.05$) or absent ($P > 0.05$). Probe sets were identified as differentially

expressed when the absolute fold change was >1.5, and the probe set was present in both samples of the relatively overexpressed group. Probe sets selected for visualization were log2 transformed and normalized to the replicate mean (estimated from basal cells). Intensity bias between the two replicates (provided to the Genomics Core Facility, MSKCC for quality control) necessitated this within replicate normalization, which leaves the data for each gene centred around zero in the basal cells.

Database accession number

Raw and normalized microarray expression data have been deposited at the Gene Expression Omnibus (GEO, http://www.ncbi.nlm.nih.gov/geo/) under the accession number GSE 25548.

Semi-quantitative RT–PCR

Equal amounts of RNAs were added to a reverse-transcriptase reaction mix (SuperScripy VILO, Invitrogen), and semi-quantitative PCR was conducted with a LightCycler system (Roche Diagnostics). Reactions were carried out using the indicated primers and template mixed with the LightCycle DNA master SYBR Green kit and run for 50 cycles. Specificity of the reactions was determined by subsequent melting curve analysis. LightCycle analysis software was used to remove background fluorescence (noise band). The number of cycles needed to reach the crossing point for each sample was used to calculate the amount of each product using the 2–CP method. Levels of PCR product were expressed as a function of peptidylprolyl isomerase D (ppid) and/or HPRT. Sequences of primers are listed in Supplementary Table S3.

Actomyosin-inhibitor treatments

E14.5 CD1 embryos were incubated with the specified concentrations of latrunculin B, Jasplakinolide, blebbistatin or DMSO (Sigma) in epidermal differentiation medium (15% fetal bovine serum, DMEM/HamsF-12 medium, 1.5 mM Ca^{2+}) at 37°C for 1 h before embedding in OCT and processing for immunofluorescence microscopy as described above.

Asymmetric cell division quantifications

Asymmetric cell division quantification was described previously[3]. Briefly, 10 μm frozen sections of E16.5 embryos were stained with DAPI to label chromatin and identify mitotic basal cells in anaphase/telophase. Following immunofluorscence processing and imaging, the angle between the basement membrane and the daughter chromatin of each anaphase basal cell was then measured. Additional sections were stained for phosphorylated histone H3 (pHH3), to mark mitotic cells, and LGN, to mark the cortical crescent that marks the orientation of one of the two spindle poles in a classical asymmetric cell division. Basal-layer early mitotic cells were first identified according to their pHH3 staining, after which their localization of LGN was determined. For these measurements, cells from three wild-type and three cKO embryos were analysed.

pHH3 quantification

Sections (10 μm) of E16.5, E17.5 and E18.5 embryos were immunostained with pHH3 and co-labelled with DAPI. The ratio between pHH3 positive cells and number of basal cells (DAPI positive) was calculated in at least ten different random fields per embryo along the back skin. For these measurements, cells from three wild-type and three cKO embryos were analysed.

Whole-mount myosin-IIA and F-actin fluorescence intensity quantifications and axial ratio calculations

Fluorescence intensity was measured in ten places along the cortex of mitotic cell and ten places in neighbouring non-mitotic cells using ImageJ software. The ratio between average intensities of mitotic versus non-mitotic cell was calculated. The raw data for these measurements were a single confocal microscopy section (0.5 μm) in the middle of the mitotic cell. The same source of data was used for axial ratio calculations, using the 'fit elipse' tool in ImageJ. For these measurements, cells from three wild-type embryos and three cKO embryos were analysed.

Immune cell quantifications

Sections (10 μm) of E16.5, E17.5 and newborn mice were immunostained with mac1, CD45 and CD3 antibodies to identify different populations of immune cells. The numbers of positive cells in the epidermis and the dermis were counted per microscopic field (×40). For these measurements, cells from three wild-type and three cKO embryos were analysed.

pERM quantification

Sections (10 μm) of E16.5 were co-labelled for LGN and pERM. Those LGN-positive cells that exhibited a continuous cortical pERM staining that was significantly brighter than neighbouring non-mitotic cells were scored as positive in our quantifications. For these measurements, cells from three wild-type and three cKO embryos were analysed.

Tissue culture, shRNA constructs and lentiviral infection

Lentiviral shRNAs (*actb*, *wdr1*) were from the TRC-1 Library (Sigma). Production of shRNA lentivirus was as described previously[63]. Epidermal keratinocytes were isolated and cultured from dispase-treated skins of wild-type CD1 mice. After replating 1×10^5 cells in a single well of a 6-well plate, cells were infected with $>10^9$ colony-forming units (c.f.u.) of lentivirus (*scramble* control or *actb* and *wdr1* shRNAs) in the presence of 100 μl polybrene. At 24 h after infection, cells were selected with 1 μg ml^{-1} puromycin (Sigma), and were plated on collagen/fibronectin-coated coverslips (75,000 cells in a single well of a 24-well plate). Eighteen hours later, cells reached ~80% confluency and were switched to differentiation media (15% fetal bovine serum, DMEM/HamsF-12 medium and 1.5 mM Ca^{2+}) supplemented with 1 μM ml^{-1} nocodazole (Sigma). For latrunculin experiments, the drug dissolved in DMSO was added 30 min before switching to high-calcium media and cultures were then fixed after 3 h. For knockdown experiments, cells were switched for 6 h and then fixed. Quantitative immunofluorescence data were collected from at least two independent experiments, in which at least 50 cells were measured per quantification using a Zeiss LSM510 laser-scanning microscope (Carl Zeiss MicroImaging) and analysed by ImageJ.

Below is information regarding TRC library shRNA constructs. (1) *Actb*, clone name: NM_007393. 1-1652s1c1 target sequence: 5′-GCATTGCTTCTGTGTAAATTA-3′; oligonucleotide sequence: 5′-CCGGGCATTGCTTCTGTGTAAATTACTCGAGTAATTTACACAGAAGCAATGCTTTTTG-3′. (2) *Actb*, clone name: NM_007393. 1-440s1c1 target sequence: 5′-CCAGATCATGTTTGAGACCTT-3′; oligonucleotide sequence: 5′-CCGGCCAGATCATGTTTGAGACCTTCTCGAGAAGGTCTCAAACATGATCTGGTTTTTG-3′. (3) *Wdr1* clone name: NM_011715. 1-1622s1c1 target sequence: 5′-GATGGCTATTCGGAGAATAAT-3′; oligonucleotide sequence: 5′-CCGGGATGGCTATTCGGAGAATAATCTCGAGATTATTCTCCGAATAGCCATCTTTTTG-3′. (4) *Wdr1* clone name: NM_011715. 1-368s1c1 target sequence: 5′-

GCTGGGAAGATCAAGGACATT-3′; oligonucleotide sequence: 5′-CCGGGCTGGGAAGATCAAGGACATTCTCGAGAATGTCCTTGATCTTCCCAGCTTTTTG-3′.

Statistics

For all quantified data, mean ± one standard deviation was presented. To determine significance between two groups, indicated in figures by an asterisk, comparisons were made using Student's *t* -test. For all statistical tests, the 0.05 level of confidence was accepted for statistical significance.

Supplementary Material

Refer to Web version on PubMed Central for supplementary material.

Acknowledgments

We thank the RU Facilities for Bioimaging (A. North) and FACS (S. Mazel) staff for their technical support; we thank N. Stokes for her assistance in the mouse facility and the Comparative Biology Center (CBC) staff for their help in veterinary care and health of our mice. We are grateful to E. Ezratty, S. Beronja, A. R. Folgueras, M. Nikolova and other members of the Fuchs laboratory for helpful discussions, critical reading of the manuscript and experimental assistance. C.L. is a Tri-Institutional Starr Stem Cell Scholars Posdoctoral Fellow. S.E.W. is an American Cancer Society Postdoctoral Fellow. Work in the Fuchs laboratory was supported by a grant from the National Institutes of Health (E.F. R01AR27883).

References

1. Blanpain C, Fuchs E. Epidermal homeostasis: a balancing act of stem cells in the skin. Nat. Rev. Mol. Cell Biol. 2009; 10:207–217. [PubMed: 19209183]
2. Perez-Moreno M, Jamora C, Fuchs E. Sticky business: orchestrating cellular signals at adherens junctions. Cell. 2003; 112:535–548. [PubMed: 12600316]
3. Lechler T, Fuchs E. Asymmetric cell divisions promote stratification and differentiation of mammalian skin. Nature. 2005; 437:275–280. [PubMed: 16094321]
4. Kunda P, Baum B. The actin cytoskeleton in spindle assembly and positioning. Trends Cell Biol. 2009; 19:174–179. [PubMed: 19285869]
5. Thery M, Bornens M. Cell shape and cell division. Curr. Opin. Cell Biol. 2006; 18:648–657. [PubMed: 17046223]
6. Carreno S, et al. Moesin and its activating kinase Slik are required for cortical stability and microtubule organization in mitotic cells. J. Cell Biol. 2008; 180:739–746. [PubMed: 18283112]
7. Kunda P, Pelling AE, Liu T, Baum B. Moesin controls cortical rigidity, cell rounding, and spindle morphogenesis during mitosis. Curr. Biol. 2008; 18:91–101. [PubMed: 18207738]
8. Thery M, et al. The extracellular matrix guides the orientation of the cell division axis. Nat. Cell Biol. 2005; 7:947–953. [PubMed: 16179950]
9. Kaji N, Muramoto A, Mizuno K. LIM kinase-mediated cofilin phosphorylation during mitosis is required for precise spindle positioning. J. Biol. Chem. 2008; 283:4983–4992. [PubMed: 18079118]
10. Cramer LP, Mitchison TJ. Investigation of the mechanism of retraction of the cell margin and rearward flow of nodules during mitotic cell rounding. Mol. Biol. Cell. 1997; 8:109–119. [PubMed: 9017599]
11. Cuenca AA, Schetter A, Aceto D, Kemphues K, Seydoux G. Polarization of the *C. elegans* zygote proceeds via distinct establishment and maintenance phases. Development. 2003; 130:1255–1265. [PubMed: 12588843]
12. Severson AF, Bowerman B. Myosin and the PAR proteins polarize microfilament-dependent forces that shape and position mitotic spindles in *Caenorhabditis elegans*. J. Cell Biol. 2003; 161:21–26. [PubMed: 12695495]

13. Munro E, Nance J, Priess JR. Cortical flows powered by asymmetrical contraction transport PAR proteins to establish and maintain anterior–posterior polarity in the early *C. elegans* embryo. Dev. Cell. 2004; 7:413–424. [PubMed: 15363415]
14. Grill SW, Gonczy P, Stelzer EH, Hyman AA. Polarity controls forces governing asymmetric spindle positioning in the *Caenorhabditis elegans* embryo. Nature. 2001; 409:630–633. [PubMed: 11214323]
15. Larson SM, et al. Cortical mechanics and meiosis II completion in mammalian oocytes are mediated by myosin-II and Ezrin–Radixin–Moesin (ERM) proteins. Mol. Biol. Cell. 2010; 15:3182–3192. [PubMed: 20660156]
16. Verdoni AM, Ikeda S, Ikeda A. Serum response factor is essential for the proper development of skin epithelium. Mamm. Genome. 2010; 21:64–76. [PubMed: 20047077]
17. Koegel H, et al. Loss of serum response factor in keratinocytes results in hyperproliferative skin disease in mice. J. Clin. Invest. 2009; 119:899–910. [PubMed: 19307725]
18. Connelly JT, et al. Actin and serum response factor transduce physical cues from the microenvironment to regulate epidermal stem cell fate decisions. Nat. Cell Biol. 2010; 12:711–718. [PubMed: 20581838]
19. Posern G, Treisman R. Actin' together: serum response factor, its cofactors and the link to signal transduction. Trends Cell Biol. 2006; 16:588–596. [PubMed: 17035020]
20. Miano JM, Long X, Fujiwara K. Serum response factor: master regulator of the actin cytoskeleton and contractile apparatus. Am. J. Physiol. Cell Physiol. 2007; 292:C70–C81. [PubMed: 16928770]
21. Miano JM, et al. Restricted inactivation of serum response factor to the cardiovascular system. Proc. Natl Acad. Sci. USA. 2004; 101:17132–17137. [PubMed: 15569937]
22. Li S, et al. Requirement for serum response factor for skeletal muscle growth and maturation revealed by tissue-specific gene deletion in mice. Proc. Natl Acad. Sci. USA. 2005; 102:1082–1087. [PubMed: 15647354]
23. Alberti S, et al. Neuronal migration in the murine rostral migratory stream requires serum response factor. Proc. Natl Acad. Sci. USA. 2005; 102:6148–6153. [PubMed: 15837932]
24. Franco CA, et al. Serum response factor is required for sprouting angiogenesis and vascular integrity. Dev. Cell. 2008; 15:448–461. [PubMed: 18804439]
25. Medjkane S, Perez-Sanchez C, Gaggioli C, Sahai E, Treisman R. Myocardin-related transcription factors and SRF are required for cytoskeletal dynamics and experimental metastasis. Nat. Cell Biol. 2009; 11:257–268. [PubMed: 19198601]
26. Vasioukhin V, Degenstein L, Wise B, Fuchs E. The magical touch: genome targeting in epidermal stem cells induced by tamoxifen application to mouse skin. Proc. Natl Acad. Sci. USA. 1999; 96:8551–8556. [PubMed: 10411913]
27. Fuchs E, Green H. Changes in keratin gene expression during terminal differentiation of the keratinocyte. Cell. 1980; 19:1033–1042. [PubMed: 6155214]
28. Coulombe PA, Kerns ML, Fuchs E. Epidermolysis bullosa simplex: a paradigm for disorders of tissue fragility. J. Clin. Invest. 2009; 119:1784–1793. [PubMed: 19587453]
29. Watt FM, Estrach S, Ambler CA. Epidermal Notch signalling: differentiation, cancer and adhesion. Curr. Opin. Cell Biol. 2008; 20:171–179. [PubMed: 18342499]
30. Rangarajan A, et al. Notch signalling is a direct determinant of keratinocyte growth arrest and entry into differentiation. EMBO J. 2001; 20:3427–3436. [PubMed: 11432830]
31. Demehri S, Kopan R. Notch signaling in bulge stem cells is not required for selection of hair follicle fate. Development. 2009; 136:891–896. [PubMed: 19211676]
32. Blanpain C, Lowry WE, Pasolli HA, Fuchs E. Canonical Notch signaling functions as a commitment switch in the epidermal lineage. Genes Dev. 2006; 20:3022–3035. [PubMed: 17079689]
33. Moriyama M, et al. Multiple roles of Notch signaling in the regulation of epidermal development. Dev. Cell. 2008; 14:594–604. [PubMed: 18410734]
34. Huang da W, Sherman BT, Lempicki RA. Systematic and integrative analysis of large gene lists using DAVID bioinformatics resources. Nat. Protoc. 2009; 4:44–57. [PubMed: 19131956]

35. Sun Q, et al. Defining the mammalian CArGome. Genome Res. 2006; 16:197–207. [PubMed: 16365378]
36. Huang QQ, et al. Role of H2-calponin in regulating macrophage motility and phagocytosis. J. Biol. Chem. 2008; 283:25887–25899. [PubMed: 18617524]
37. Hossain MM, Smith PG, Wu K, Jin JP. Cytoskeletal tension regulates both expression and degradation of h2-calponin in lung alveolar cells. Biochemistry. 2006; 45:15670–15683. [PubMed: 17176089]
38. Hossain MM, Crish JF, Eckert RL, Lin JJ, Jin JP. h2-Calponin is regulated by mechanical tension and modifies the function of actin cytoskeleton. J. Biol. Chem. 2005; 280:42442–42453. [PubMed: 16236705]
39. Feng Y, Walsh CA. The many faces of filamin: a versatile molecular scaffold for cell motility and signalling. Nat. Cell Biol. 2004; 6:1034–1038. [PubMed: 15516996]
40. Fujibuchi T, et al. AIP1/WDR1 supports mitotic cell rounding. Biochem. Biophys. Res. Commun. 2005; 327:268–275. [PubMed: 15629458]
41. Fang M, et al. Evidence of EGR1 as a differentially expressed gene among proliferative skin diseases. Genomic. Med. 2007; 1:75–85. [PubMed: 18923931]
42. Kumbrink J, Kirsch KH, Johnson JP. EGR1, EGR2, and EGR3 activate the expression of their coregulator NAB2 establishing a negative feedback loop in cells of neuroectodermal and epithelial origin. J. Cell Biochem. 2010; 111:207–217. [PubMed: 20506119]
43. Kubosaki A, et al. Genome-wide investigation of *in vivo* EGR-1 binding sites in monocytic differentiation. Genome Biol. 2009; 10:R41. [PubMed: 19374776]
44. Thyss R, et al. NF-κB/Egr-1/Gadd45 are sequentially activated upon UVB irradiation to mediate epidermal cell death. EMBO J. 2005; 24:128–137. [PubMed: 15616591]
45. Thery M, Bornens M. Get round and stiff for mitosis. Hfsp J. 2008; 2:65–71. [PubMed: 19404473]
46. Morton WM, Ayscough KR, McLaughlin PJ. Latrunculin alters the actin-monomer subunit interface to prevent polymerization. Nat. Cell Biol. 2000; 2:376–378. [PubMed: 10854330]
47. Ayscough KR, et al. High rates of actin filament turnover in budding yeast and roles for actin in establishment and maintenance of cell polarity revealed using the actin inhibitor latrunculin-A. J. Cell Biol. 1997; 137:399–416. [PubMed: 9128251]
48. Siller KH, Doe CQ. Spindle orientation during asymmetric cell division. Nat. Cell Biol. 2009; 11:365–374. [PubMed: 19337318]
49. Neumuller RA, Knoblich JA. Dividing cellular asymmetry: asymmetric cell division and its implications for stem cells and cancer. Genes Dev. 2009; 23:2675–2699. [PubMed: 19952104]
50. Zheng Z, et al. LGN regulates mitotic spindle orientation during epithelial morphogenesis. J. Cell Biol. 2010; 19:275–288. [PubMed: 20385777]
51. Morin X, Jaouen F, Durbec P. Control of planar divisions by the G-protein regulator LGN maintains progenitors in the chick neuroepithelium. Nat. Neurosci. 2007; 10:1440–1448. [PubMed: 17934458]
52. Konno D, et al. Neuroepithelial progenitors undergo LGN-dependent planar divisions to maintain self-renewability during mammalian neurogenesis. Nat. Cell Biol. 2008; 10:93–101. [PubMed: 18084280]
53. Bubb MR, Senderowicz AM, Sausville EA, Duncan KL, Korn ED. Jasplakinolide, a cytotoxic natural product, induces actin polymerization and competitively inhibits the binding of phalloidin to F-actin. J. Biol. Chem. 1994; 269:14869–14871. [PubMed: 8195116]
54. Straight AF, et al. Dissecting temporal and spatial control of cytokinesis with a myosin II inhibitor. Science. 2003; 299:1743–1747. [PubMed: 12637748]
55. Effler JC, et al. Mitosis-specific mechanosensing and contractile-protein redistribution control cell shape. Curr. Biol. 2006; 16:1962–1967. [PubMed: 17027494]
56. Cabernard C, Prehoda KE, Doe CQ. A spindle-independent cleavage furrow positioning pathway. Nature. 2010; 467:91–94. [PubMed: 20811457]
57. Knoblich JA. Mechanisms of asymmetric stem cell division. Cell. 2008; 132:583–597. [PubMed: 18295577]

58. Ou G, et al. Polarized myosin produces unequal-size daughters during asymmetric cell division. Science. 2010; 330:677–680. [PubMed: 20929735]

59. Li R, Gundersen GG. Beyond polymer polarity: how the cytoskeleton builds a polarized cell. Nat. Rev. Mol. Cell Biol. 2008; 9:860–873. [PubMed: 18946475]

60. Chai J, Tarnawski AS. Serum response factor: discovery, biochemistry, biological roles and implications for tissue injury healing. J. Physiol. Pharmacol. 2002; 53:147–157. [PubMed: 12120892]

61. Srinivas S, et al. Cre reporter strains produced by targeted insertion of EYFP and ECFP into the ROSA26 locus. BMC Dev. Biol. 2001; 1:4. [PubMed: 11299042]

62. Vasioukhin V, Fuchs E. Actin dynamics and cell–cell adhesion in epithelia. Curr. Opin. Cell Biol. 2001; 13:76–84. [PubMed: 11163137]

63. Beronja S, Livshits G, Williams S, Fuchs E. Rapid functional dissection of genetic networks via tissue-specific transduction and RNAi in mouse embryos. Nat. Med. 2010; 16:821–827. [PubMed: 20526348]

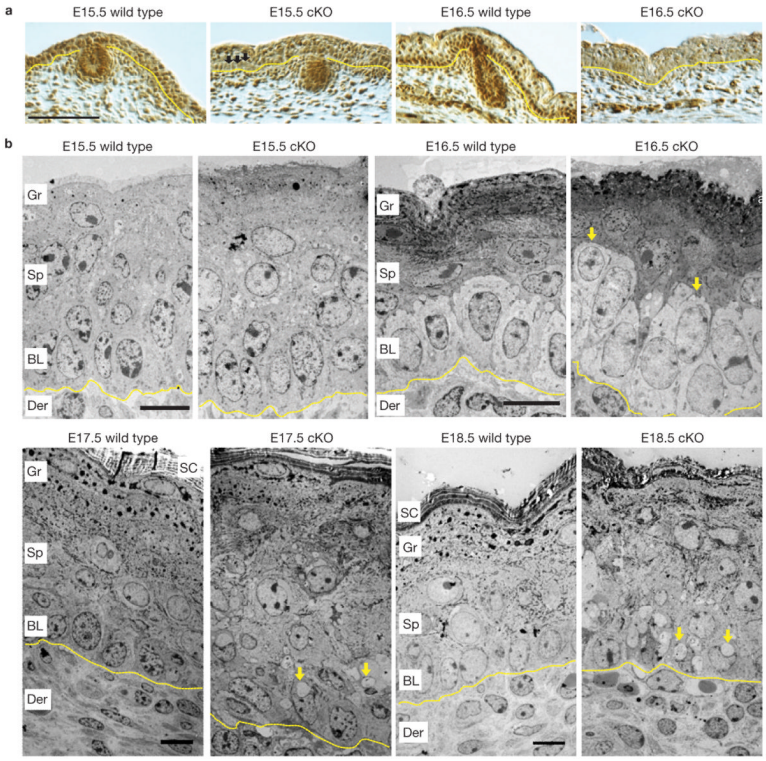

Figure 1.

Srf is expressed in embryonic basal cells and when absent, morphological abnormalities originate at the basal to suprabasal juncture. (**a**) Anti-Srf immunohistochemistry of skins of *Srf-cKO* and wild-type littermate embryos at embryonic ages indicated. Nuclear Srf is lost in some *Srf-cKO* basal cells by E15.5 (arrows), but in nearly all basal cells by E16.5, when Srf is strongly expressed in the wild-type basal layer. Scale bar,100 μm. (**b**) Corresponding transmission electron micrographs of ultrathin sections of back-skin epidermis. Arrows in E16.5-cKO skin denote cells with basal morphology that seem to be suprabasal. Arrows in E17.5- and E18.5-cKO skin indicate vacuoles not seen in normal epidermis. Note also that the basal–suprabasal demarcation is completely disrupted by E17.5. Der, dermis; BL, basal layer; Sp, spinous layer; Gr, granular layer; SC, stratum corneum. Dotted lines denote dermal–epidermal boundary. Scale bars,10 μm.

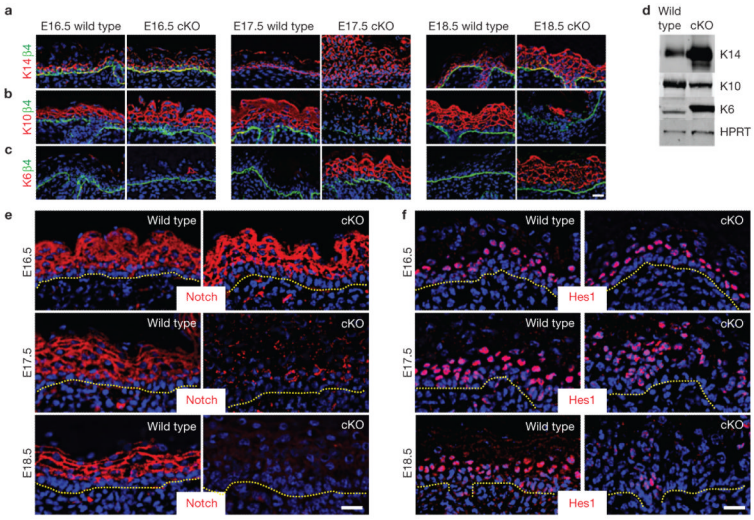

Figure 2.

Alterations in biochemical markers of the basal–suprabasal switch are obvious by E17.5 in *Srf* -null epidermis. Immunofluorescence microscopy and/or immunoblot analyses of *Srf*-cKO and wild-type skins at ages indicated. Colour-coding is according to secondary antibodies used. (**a**,**b**) Basal markers β4-integrin and K14 and spinous layer differentiation marker K10 reveal disruption in the basal–suprabasal switch by E17.5. (**c**) K6 is known to be induced in spinous cells whenever there is an imbalance in epidermal homeostasis, as revealed here at E17.5 in *Srf* -null epidermis. (**d**) Immunoblot of total epidermal lysates from newborn epidermis probed with the same antibodies as in **a**–**c** and also hypoxanthine phosphoribosyl-transferase (HPRT, control). (**e**,**f**) Notch signalling, another sign of the basal–suprabasal switch, is also markedly perturbed in E17.5 *Srf*-cKO skin, as evidenced by diminished Notch3 and a Notch target Hes1. Dotted lines denote dermal–epidermal boundary. Scale bars,20 μm. Uncropped images of blots are shown in Supplementary Fig. S9.

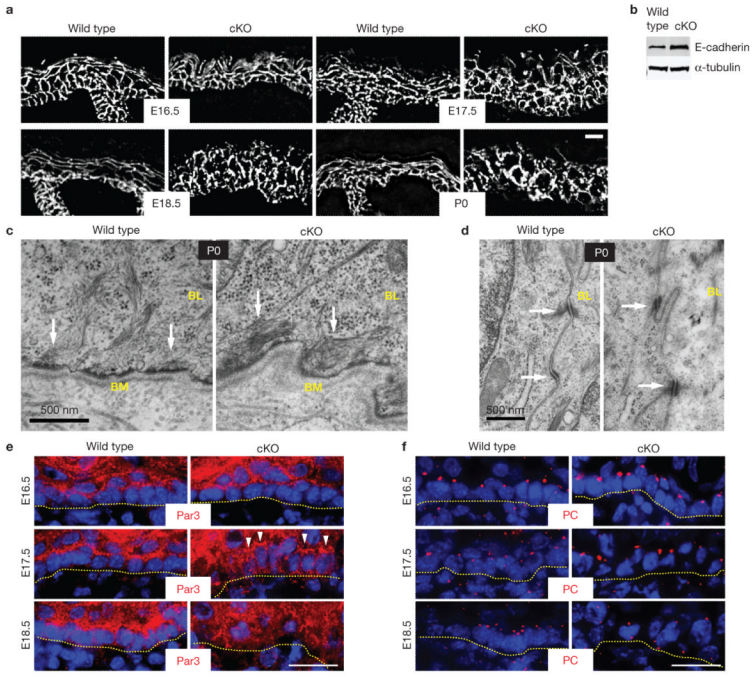

Figure 3.

Cell adhesion remains intact during embryonic development in *Srf*-cKO skin. (**a**) Despite alterations in epidermal architecture in the absence of Srf, E-cadherin immunofluorescence was localized at sites of cell–cell contacts throughout development. Scale bar,20 μm. (**b**) Immunoblot analyses of total epidermal lysates from newborn pups. (**c**,**d**) Ultrastructural analyses of newborn epidermis reveals no major differences in cellular junctions between wild-type and *Srf*-cKO. **c** shows hemidesmosomes and **d** shows desmosomes, both readily identified by their electron density and their attachment to keratin filament bundles (arrows). The basement membrane (BM) is the electron dense line directly beneath the epidermis. BL, basal layer. Scale bar,500 nm. (**e**,**f**) Immunofluorescence microscopy of wild-type and *Srf*-cKO skins, labelled for ABP markers. In wild-type basal cells, Par3 is enriched at the apical cortex and the centrosomal marker Pericentrin (PC) is localized apically. As judged by these markers and in agreement with ultrastructure, *Srf*-cKO-mediated perturbations in ABP were first evident at E17.5, although many cells still showed normal distribution of these markers (arrowheads). Dotted lines denote dermal–epidermal boundary. Scale bar,20 μm. Uncropped images of blots are shown in Supplementary Fig. S9.

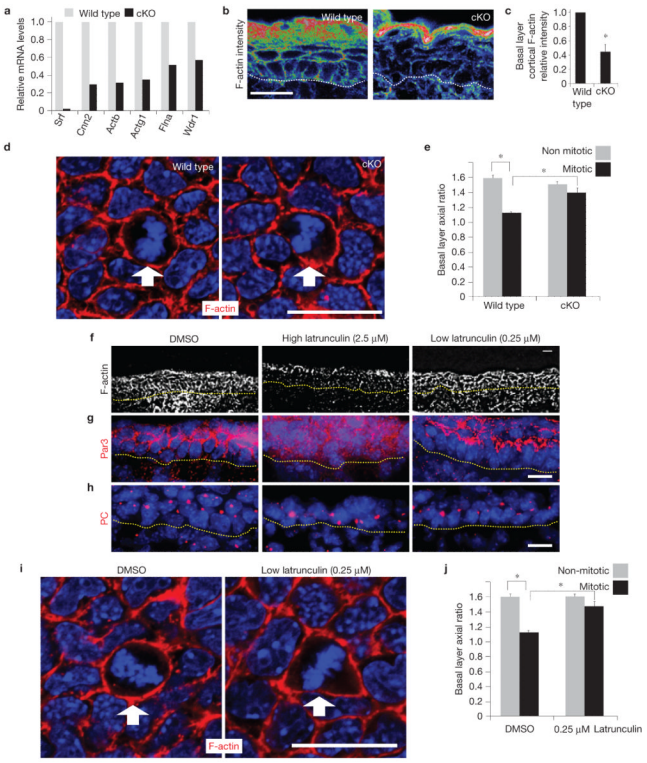

Figure 4.

Conditional *Srf* ablation results in an early reduction in cortical actin, which seems to be directly responsible for an associated ability of early mitotic cells to round up during mitosis. (**a**) Verification of the array results on actin genes from Table 1. qPCR of mRNAs are from FACS-purified E16.5 basal progenitors. *n*=2. (**b**,**c**) Confocal microscopy and fluorescence intensity quantifications of phalloidin-stained E16.5 skin sections; warmer-coloured pixels indicate higher fluorescence intensity. Basal cell cortical F-actin intensity is significantly decreased in *Srf*-cKO versus wild-type counterparts (* indicates P=0.013,n=3). (**d**,**e**) Whole-mount fluorescence microscopy of E16.5 embryos labelled for F-actin and DAPI and imaged in the plane of the basal layer. Note: cKO image was exposed longer than wild type, to visualize cortical actin and cell shape. Quantifications are of the axial ratios of interphase versus early mitotic (prophase to metaphase) cells, which are reduced in wild-type, but not in *Srf*-cKO, embryos (* indicates P< 0.05,n=3; wild-type interphase versus early mitotic cells, P =0.004; wild-type versus *Srf*-cKO early mitotic cells, P =0.02). (**f**–**j**) F-actin inhibitor defects are similar to Srf loss of function. Although exposure of mouse embryos to 2.5 μM latrunculin for 1 h disrupted ABP, exposure to 0.25 μM did not (**f**–**h**). Under these milder conditions, early mitotic basal cells failed to round up properly, as imaged by whole-mount fluorescence microscopy (**i**) and as quantified by measuring the axial ratios of interphase versus early mitotic (prophase to metaphase) cells (**j**) (* indicates P <0.05,n=3; DMSO (control) interphase versus early mitotic cells, P =0.0003; DMSO versus 0.25 μM latrunculin in early mitotic cells, P =0.008). Dotted line denotes dermal–epidermal border. Arrow denotes early mitotic cell. Error bars represent s.d. Scale bar,20 μm.

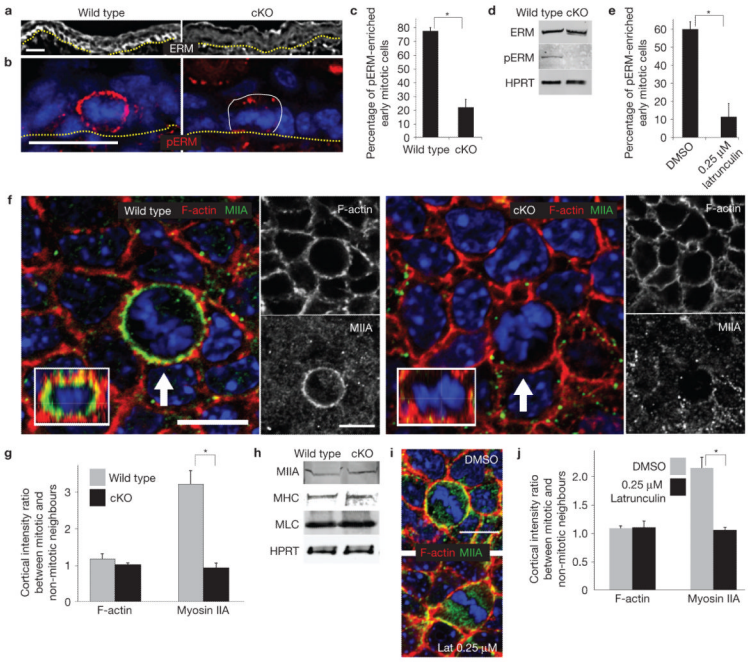

Figure 5.

Srf-cKO early mitotic cells are defective in enriching and activating ERM proteins at the actin cortex and in recruiting myosin-IIA. (**a**,**b**) Immunofluorescence microscopy of E16.5 epidermis reveals an enrichment of cortically localized ERM in the basal layer and activation (phosphorylation) of ERM (pERM) in early mitotic cells. Both are perturbed in *Srf*-cKO skin. Dotted lines denote dermal–epidermal border. Thin line denotes boundary of mitotic cell at right. Scale bars,20 μm. (**c**) Quantifications reveal a threefold decrease in pERM (* indicates P =0.0007,n=3) at the cortex of early mitotic basal cells. (**d**) Immunoblot analyses=of total epidermal lysates. HPRT, hypoxanthine phosphoribosyl-transferase loading control. Note that despite reduction in ERM at basal cortex, overall levels of ERM seem to be similar. Note also that ERM activation is clearly reduced following Srf deficiency. (**e**) Treatment with 0.25 μM latrunculin achieves a similar effect to Srf deficiency with respect to pERM enrichment at the cortex of early mitotic cells (* indicates P =0.002,n=3). (**f**,**g**) Planar images are through the basal layer of E16.5 embryos, subjected to whole-mount fluorescence microscopy for F-actin (phalloidin), myosin-IIA and DAPI. Arrows indicate early mitotic cells, enriched in myosin-IIA in wild type, but not *Srf*-cKO. Insets, reconstructed X –Z view of the compressed Z -stack images to show that myosin-IIA is enriched throughout the cortex of wild-type, but not cKO, mitotic cells. Scale bars,10 μm. (**g**) Quantifications of fluorescence intensity ratios of F-actin and myosin-IIA from mitotic versus non-mitotic cells. * indicates P =0.0066,n=3. (**h**) Immunoblot analyses of total newborn epidermal lysates. Blots were probed with antibodies against myosin-IIA, pan-myosin heavy chain (MHC), myosin light chain (MLC) and HPRT. (**i**,**j**) E14.5 embryos were treated with DMSO or 0.25 μM latrunculin and stained for F-actin, myosin-IIA and DAPI. Shown are planar views of basal layer and quantifications of fluorescence intensity ratios of F-actin and myosin-IIA in mitotic versus neighbouring non-mitotic cells. indicates P =0.008,n=3. Scale bar,10 μm error bars represent s.d. Uncropped images of blots are shown in Supplementary Fig. S9.

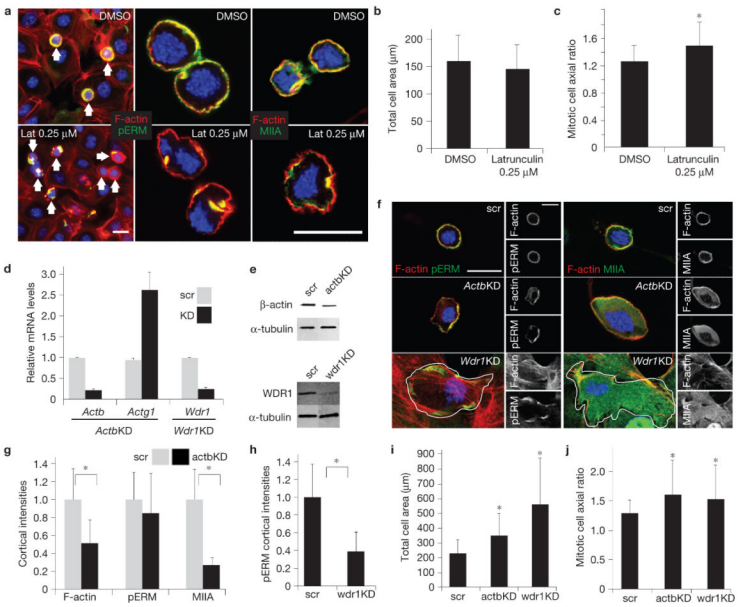

Figure 6.

Actin and actin regulators downregulated in Srf-deficient basal cells are required for keratinocytes to undergo proper cortical and cell shape changes during mitosis. Epidermal monolayers of cultured wild-type keratinocytes were treated with either DMSO, 0.25 μM latrunculin for 30 min or lentiviruses harbouring *Actb*, *Wdr 1* or scramble shRNAs, as described in the text. Following treatment with calcium to promote adhesion and stratification and nocodazole to arrest cells in mitosis, cultures were then fixed and labelled for F-actin (red), pERM or myosin-IIA (MIIA, green) and DAPI to mark chromatin (blue). (**a**) DMSO- and latrunculin-treated cultures; note cortical enrichment of pERM and myosin-IIA in DMSO-treated mitotic cells, but the diminished distribution of pERM and myosin-IIA in latrunculin-treated mitotic cells. Arrows denote mitotic cells. (**b**,**c**) Morphometric quantifications of mitotic cells revealed normal total area (**b**), but increased axial ratio (**c**) in latrunculin-treated cells (* denotes P =0.0005). (**d**) Real-time PCR to measure mRNA levels of *Actb*, *Actg1* and *Wdr1* in the lentiviral-transduced cultures indicated (KD, knockdown; scr, scramble). (**e**) Immunoblots were probed with antibodies against β-actin, Wdr1 and α-tubulin. (**f**) Cell morphology, pERM, cortical actin and/or myosin-IIA are perturbed in keratinocytes expressing *Actb* or *Wdr 1* shRNAs, but not scramble control. White lines denote cell borders. (**g**) Cortical fluorescence intensity quantifications in *Actb*-knockdown cells reveal significant decreases in cortical actin and myosin-IIA intensities (* denotes P <0.05; F-actin intensity in scramble versus *Actb* knockdown, $P=9.4\times10^{-7}$; myosin-IIA intensity in scramble versus *Actb* knockdown, $P = 9.03\times10^{-10}$). (**h**) Cortical fluorescence intensity quantifications in *Wdr 1*-knockdown cells reveal significant decreases in pERM intensity (* denotes $P = 1.69\times10^{-14}$). (**i**) Quantifications of total mitotic cell areas reveal significant increases in both *Actb*- and *Wdr 1*-knockdown mitotic cells (* denotes P <0.05; scramble versus *actb* knockdown, $P = 1.07\times10^{-6}$; scramble versus *Wdr 1* knockdown $P=6.1\times10^{-7}$). (**i**) Quantifications of mitotic cell axial ratios reveal a significant increase on both *Actb*- and *Wdr 1*-knockdown (* denotes $P < 0.05$; scramble versus *Actb* knockdown, P = 0.0003; scramble versus *Wdr 1* knockdown, P =0.024). Scale bars,20 μm for all quantifications $n \geq 50$. error bars represent s.d. Uncropped images of blots are shown in Supplementary Fig. S9.

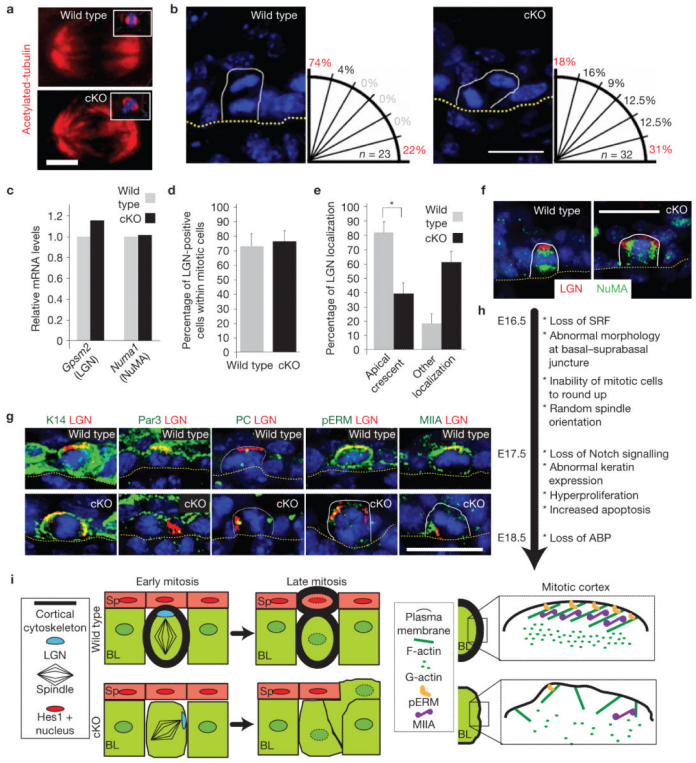

Figure 7.

Mitotic abnormalities in spindle orientation and LGN–NuMA localization in E16.5 *Srf*-cKO basal cells. (**a**) Representative immunofluorescence micrographs depicting seemingly normal spindles from early mitotic cells of E16.5 embryos. Anti-acetylated tubulin was used to visualize the spindle and DAPI to mark chromatin. Insets show reconstructed *X* –*Z* view. Scale bar,2 μm. (**b**) DAPI staining highlights anaphase/telophase chromatin and reveals the angle between daughter nuclei in mitotic basal keratinocytes of E16.5 embryos. To the right of each representative image is a schematic showing the quantifications of spindle plane (*n*, number of anaphase/telophase cells analysed), measured relative to the underlying basement membrane (dotted line) delineating the epidermal-dermal boundary. Scale bar,20 μm. (**c**) qPCR analysis for mRNA levels of G-protein signalling modulator 2 (*Gpsm2* ; LGN) and *Numa1* (NuMA). (**d**,**e**) Quantifications of mitotic E16.5 basal cells revealing similar percentages of early mitotic cells (pHH3+) in which LGN can be detected by immunolabelling (**d**), but perturbations in the normal apical cortical localization of LGN in mitotic cells (**e**; * indicates *P* =0 001,n =3). (**f**) Representative immunofluorescence micrographs of mitotic basal cells labelled for LGN and NuMA. Scale bar,20 μm. (**g**) LGN mislocalization is concomitant with pERM and myosin-IIA abnormalities, but precedes aberrations in apical Par3. Colour-coding is according to secondary antibodies used. Scale bar,20 μm. (**h**) A summary of the temporal progression of the *Srf*-cKO phenotype. (**i**) Working model consistent with the data presented. BL, basal layer; Sp, spinous layer.

Table 1

Most early transcriptional changes in basal cells depleted of Srf involve regulators of actomyosin and not cell cycle, inflammation, ABP or Notch signalling genes.

Actomyosin cytoskeleton	*Fblim1(−3.7)** *Cnn2(−3.1)** *Actb(−2.0)** *Flna(−1.8)** *Arhgap24(−1.8)** *Actg1(−1.7)** *Wdr1(−1.6)** *Pfn2(−1.3)** *Gsn(−1.3)** *Myh9*† *Myh10*† *Myh14*† *Myl9*†
Cell adhesion	*Gjb5(−2.6)** *Pcad20(−2.2)** *Dsg1b(−1.8)** *Tns4(−1.6)** *Cdh1*† *Ctnna1*† *Ctnnb1*† *Tjp1*† *Tjp2*† *Ocln*† *Itgb1*†
Immediate early genes	*Egr2(−8.6)** *Egr1(−5.0)** *Egr3(−3.9)** *Fos*† *Junb*†
Immune response	*Il1b*† *Il6*† *Il18*† *Ccl2*† *Ccl27a*† *S100a8*† *S100a9*†
Cell cycle	*Mki67*† *Ccna1*† *Ccna2*† *Ccnb1*† *Ccnb2*† *Ccnd1*† *Ccnd2(1.5)*‡ *Ccnd3*† *Ccne1*† *Ccne2*†
Notch signalling	*Notch1*† *Notch2*† *Notch3*† *Jag1*† *Jag2* † *Dll1*†
Apico-basal polarity	*Pard3*† *Pard3b*† *Pard6a*† *Pard6b*† *Pard6g* † *Prkcc*† *Prkcz*†

Embryos were from *K*14–*Cre*×*Rosa*26*YFP fl/fl* ×*Srf fl/fl* (wild-type and cKO littermates). Basal cells active for Cre recombinase expressed YFP and were enriched for surface α6-integrin. After FACS purification, mRNAs were subjected in duplicate for microarray analyses. Data from two independent arrays revealed 72 mRNAs that scored as up- or downregulated by at least 1.5-fold with $P < 0.05$. DAVID clustering analyses showed that the affected process is the actomyosin cytoskeleton, whereas ABP, Notch, cell cycle regulators and pro-inflammation associated genes showed no change at this early time.

* Decrease in early (E16.5) mRNA expression

† No change in early (E16.5) mRNA expression

‡ Increase in early (E16.5) mRNA expression

Nat Cell Biol. Author manuscript; available in PMC 2012 February 13.